JOURNAL OF COMPUTATIONAL PHYSICS 91, 71–93 (1990)

A New Optimized FCT Algorithm for Shock Wave Problems*

DUŠAN ODSTRČIL

Geophysical Institute, Slovak Academy of Sciences, Dúbravská cesta 9, 84228 Bratislava, Czechoslovakia

Received September 7, 1988; revised August 7, 1989

The new XDFCT algorithm is presented for the solution of hydrodynamic flow problems with steep gradients. This algorithm is an explicit finite-difference scheme based on the flux-corrected transport technique and it is a modification of existing ETBFCT algorithm. The use of different diffusive and antidiffusive fluxes enables us to use twice the time step with similar accuracy. This is shown by linear numerical analysis and verified by solution of three test problems. © 1990 Academic Press, Inc.

1. INTRODUCTION

In many practical situations hydrodynamic flow occurs with steep gradients such as shock waves and contact discontinuities. High accuracy in the numerical solution of such problems is often of a primary interest. Among the most general and accurate methods of solution are explicit finite-difference schemes which use the flux-corrected transport technique [1, 2]. These algorithms require no knowledge about the character of solution, are not restricted to a specific class of problems, and are independent of the use of various equations of state for different fluids.

In this paper we attempt to optimize the well-known ETBFCT algorithm [3, 4] which is considered to be one of the best of the above-mentioned algorithms. First, we present a linear numerical analysis of FCT algorithms and show the possibility of their optimization by modification of the diffusive and antidiffusive fluxes. This modification is named the XDFCT algorithm. Then we introduce three test problems to judge the influence of our modifications as well as for comparison with other algorithms. Solution of the given test problems verifies the possibility of using twice the time step with similar accuracy.

2. NUMERICAL APPROXIMATION

Partial differential equations describing hydrodynamic flow may be approximated by a difference scheme on a discrete mesh. Values of variables are defined on

* Work performed while the author was at the Occupational Safety Research Institute, Obrancov mieru 47, 81435 Bratislava, Czechoslovakia

0021-9991/90 $3.00

the mesh at the discrete time levels t^n as averaged values within each mesh cell j with centers at the positions x_j and interfaces at the positions $x_{j+1/2}$. Basic properties of the difference scheme and errors in the resulting solution can be studied by means of linear numerical analysis (see the Appendix for more details). For simplicity, the continuity equation

$$\frac{\partial}{\partial t}(\rho)+\frac{\partial}{\partial x}(\rho v)=0, \tag{1}$$

where ρ is the density and v is the constant velocity, will be used in what follows.

2.1. *The FCT Difference Scheme*

The solution of Eq. (1) by the FCT technique may be symbolically written as

$$\rho_j^{n+1}=\rho_j^n-\frac{f_{j+1/2}^{\mathrm{T}}-f_{j-1/2}^{\mathrm{T}}}{\Delta x}+\frac{f_{j+1/2}^{\mathrm{D}}-f_{j-1/2}^{\mathrm{D}}}{\Delta x}-\frac{f_{j+1/2}^{\mathrm{A}}-f_{j-1/2}^{\mathrm{A}}}{\Delta x}, \tag{2}$$

where f^{T} are the transport fluxes which reflect the real transport of mass, f^{D} are the diffusive fluxes which introduce a numerical diffusion to the solution in order to ensure the stability and monotonicity, and f^{A} are the antidiffusive fluxes which eliminate the excessive numerical diffusion where it is possible. The solution is, in fact, obtained by subsequent steps and the amount of antidiffusive fluxes is controlled by the limiter to avoid formation of new maxima or minima [4, 5]. The usage of fluxes ensures the conservation property, because the same values are used as input for one cell and as output for an adjacent cell.

The transport fluxes f^{T} may be written as

$$f_{j+1/2}^{\mathrm{T}}=\tfrac{1}{2}(\rho_{j+1}^n+\rho_j^n)\,v\,\Delta t, \tag{3}$$

and after their application, the density values are

$$\rho_j^{\mathrm{T}}=\rho_j^n-\frac{\varepsilon}{2}(\rho_{j+1}^n-\rho_{j-1}^n), \tag{4}$$

where $\varepsilon=v(\Delta t/\Delta x)$ is the Courant number. This difference scheme is known as the forward time centered space (FTCS) scheme and the resulting solution is named as the transported solution. However, it can be shown that this scheme is unstable.

The numerical stability is obtained by the addition of a diffusion term to the transported solution. This may be done by introducing the diffusive fluxes

$$f_{j+1/2}^{\mathrm{D}}=d\frac{\rho_{j+1}^n-\rho_j^n}{\Delta x}, \tag{5}$$

where $d>0$ is the artificial viscosity coefficient. The resulting solution is named the transported diffused solution and may be written as

$$\rho_j^{\mathrm{TD}}=\rho_j^{\mathrm{T}}+\nu(\rho_{j+1}^n-2\rho_j^n+\rho_{j-1}^n), \tag{6}$$

where $v = d/(\Delta x)^2$ is the diffusion coefficient. It can be shown that the solution is stable for

$$|\varepsilon| \leqslant 1 \tag{7}$$

and

$$v \geqslant \tfrac{1}{2}\varepsilon^2. \tag{8}$$

The use of small values of the diffusion coefficient gives a nonmonotonic solution (i.e., it contains unphysical oscillations near steep gradients). It was shown [1] that monotonicity is ensured if

$$\tfrac{1}{2}|\varepsilon| \leqslant v \leqslant \tfrac{1}{2}. \tag{9}$$

For $|\varepsilon| < 1$, the value of $\frac{1}{2}|\varepsilon|$ is always larger than the value of $\frac{1}{2}\varepsilon^2$ as is shown in Fig. 1. Thus for ensuring monotonicity a higher numerical diffusion has to be used than it is sufficient for ensuring stability. However, whether the monotonicity

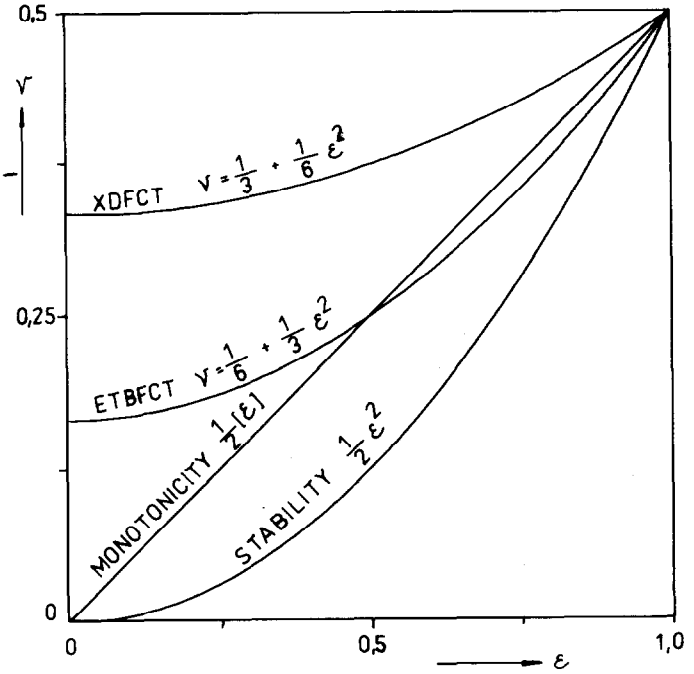

FIG. 1. Diffusion coefficients v of the ETBFCT and XDFCT algorithms, stability condition (8), and monotonicity condition (9) as functions of the Courant number $\varepsilon = v(\Delta t/\Delta x)$. While the ETBFCT is limited by $|\varepsilon| < \frac{1}{2}$ to obtain monotonic solution the XDFCT is limited by $|\varepsilon| < 1$ and thus it can use twice the time step.

will be really violated depends on the specific situation for each cell of the mesh. Therefore a more accurate solution can be obtained by elimination or reduction of this excessive diffusion if it occurs. This is principle of the FCT technique and this task is performed by the antidiffusive fluxes controlled by the limiter [4, 5].

2.2. *The Original FCT Algorithms*

The first FCT algorithms has been the SHASTA [5] and it uses the antidiffusive fluxes,

$$f^{\mathrm{A}}_{j+1/2} = a\,\frac{\rho^{\mathrm{TD}}_{j+1} - \rho^{\mathrm{TD}}_{j}}{\Delta x}, \tag{10}$$

where $a > 0$, and the antidiffusion coefficient is defined as $\mu = a/(\Delta x)^2$. However, when the velocity is zero, it is not possible to eliminate diffusion (known as the residual diffusion).

Therefore this algorithm has been subsequently modified using the antidiffusive fluxes,

$$f^{\mathrm{A}}_{j+1/2} = a\,\frac{\rho^{\mathrm{T}}_{j+1} - \rho^{\mathrm{T}}_{j}}{\Delta x}. \tag{11}$$

Such an algorithm has been named as the low phase error (LPE) phoenical FCT algorithm [1, 8] and its generalization to various coordinate systems and non-Eulerian meshes has been named as the ETBFCT algorithm [3, 4]. Linear numerical analysis of the difference scheme gives the amplification function,

$$g = 1 - 2(v-\mu)(1-\cos\beta) - i\varepsilon[(1+2\mu)\sin\beta - \mu\sin 2\beta], \tag{12}$$

the relative amplitude error,

$$A = [2(v-\mu) - \varepsilon^2]\,\beta^2 + \left[-(v-\mu)^2 - \frac{v-\mu}{6} + \frac{1}{3}\varepsilon^2 - 2\mu\varepsilon^2\right]\beta^4 + \cdots, \tag{13}$$

and the relative phase error,

$$R = (v - \tfrac{1}{6} - \tfrac{1}{3}\varepsilon^2)\,\beta^2 + O(\beta^4) + \cdots. \tag{14}$$

From (12) it can be seen that for $\varepsilon = 0$ the amplification functions equals one (i.e., there is no residual diffusion) if $v = \mu$. In addition, choosing

$$v = \tfrac{1}{6} + \tfrac{1}{3}\varepsilon^2 \tag{15}$$

$$\mu = \tfrac{1}{6} - \tfrac{1}{6}\varepsilon^2 \tag{16}$$

enables fulfillment of the condition for zero residual diffusion and simultaneously reduces both amplitude and phase errors to the fourth order. Though the difference scheme is stable for $|\varepsilon| \leqslant 1$, using the above diffusion and antidiffusion coefficients

restricts its application for $|\varepsilon| \leqslant \frac{1}{2}$. This is caused by violation of the monotonicity condition (9) for $\frac{1}{2} < |\varepsilon| < 1$ (see Fig. 1).

2.3. *The XDFCT Algorithm*

The occurrence of the residual diffusion in the SHASTA algorithm when the velocity is zero is understandable. Its antidiffusive fluxes use the ρ^{TD} values which are always different from the original values ρ^n used for the diffusive fluxes. Thus the antidiffusion is not able to fully remove the introduced diffusion. On the other hand, there is no transport when the velocity is zero ($\rho^T \equiv \rho^n$) and the ETBFCT algorithm uses the same values for the diffusive and antidiffusive fluxes. Thus it is possible to fully eliminate the residual diffusion.

We note that the values of ρ^T are not the only ones which remain unchanged by the difference scheme when the velocity is zero. The phoenical antidiffusive fluxes can also be obtained using the values of ρ^n or $\rho^{n+1/2}$.

Using ρ^n gives no advantage, because then the diffusive and antidiffusive fluxes are the same except for the different coefficients used. Thus these coefficients are not independent and one value is actually used in the amplification function. Therefore it is not possible to minimize both the amplitude and phase errors.

However, using $\rho^{n+1/2}$ is more promising. As with the ETBFCT, the diffusive and antidiffusive fluxes use the same density gradients when the velocity is zero and they are independent in a general case. The values of $\rho^{n+1/2}$ are calculated at the auxiliary "half" time step. This step is redundant for the other FCT algorithms when the passive convection with a constant velocity is calculated. In general, however, they also use the half step because the transport fluxes have to be time centered. While the other FCT algorithms can use the same difference scheme for both steps, using the atidiffusive fluxes with $\rho^{n+1/2}$ prevents this. The ETBFCT difference scheme is used to gain $\rho^{n+1/2}$ during the half time step,

$$\rho_j^{n+1/2} = \rho_j^n - \frac{\varepsilon}{4}(\rho_{j+1}^n - \rho_{j-1}^n) + \nu(\rho_{j+1}^n - 2\rho_j^n + \rho_{j-1}^n) - \mu(\rho_{j+1}^T - 2\rho_j^T + \rho_{j-1}^T), \quad (17)$$

where

$$\rho_j^T = \rho_j^n - \frac{\varepsilon}{4}(\rho_{j+1}^n - \rho_{j-1}^n) \quad (18)$$

and ν and μ are the diffusion and antidiffusion coefficients used at the half step. Then ρ^{n+1} can be calculated by a second difference scheme during the full time step,

$$\rho_j^{n+1} = \rho_j^n - \frac{\varepsilon}{2}(\rho_{j+1}^n - \rho_{j-1}^n) + N(\rho_{j+1}^n - 2\rho_j^n + \rho_{j-1}^n) - M(\rho_{j+1}^{n+1/2} - 2\rho_j^{n+1/2} + \rho_{j-1}^{n+1/2}), \quad (19)$$

where N and M are the diffusion and antidiffusion coefficients used at the full step.

The above given two step difference scheme has been named the XDFCT. Its numerical analysis is given in the Appendix in more detail. The XDFCT difference scheme has the amplification function,

$$g = 1 - 2(N-M)(1-\cos\beta) - 2M(\nu-\mu)(\cos 2\beta - 4\cos\beta + 3) - i\varepsilon\left[\left(1+M+\frac{5}{2}M\mu\right)\sin\beta - \left(\frac{M}{2}+2M\mu\right)\sin 2\beta + \frac{M\mu}{2}\sin 3\beta\right], \quad (20)$$

the relative amplitude error,

$$A = [2(N-M)-\varepsilon^2]\,\beta^2 + \left[-(N-M)^2 - \frac{N-M}{6} + 2M(\nu-\mu) + \frac{1}{3}\varepsilon^2 - M\varepsilon^2\right]\beta^4 + \cdots, \quad (21)$$

and the relative phase error,

$$R = \left(N - \frac{M}{2} - \frac{1}{6} - \frac{1}{3}\varepsilon^2\right)\beta^2 + O(\beta^4) + \cdots. \quad (22)$$

From (20) it can be seen that for $\varepsilon = 0$ the amplification function equals one (i.e., there is no residual diffusion) if $\nu = \mu$ and $N = M$. Further, choosing the following diffusion and antidiffusion coefficients,

$$N = \tfrac{1}{3} + \tfrac{1}{6}\varepsilon^2 \quad (23)$$

$$M = \tfrac{1}{3} - \tfrac{1}{3}\varepsilon^2, \quad (24)$$

enables us to fulfill the condition of zero residual diffusion and to reduce simultaneously both amplitude and phase errors to the fourth order. Thus XDFCT has error properties similar to those of ETBFCT. However, the larger diffusion coefficients ensure the monotonicity for $|\varepsilon| \leqslant 1$ (Fig. 1). This enables us to use twice the time step in calculations.

3. Test Problems

We have chosen three test problems for a thorough comparison of our modifications of the ETBFCT algorithm. These tests have been already published together with the exact solutions. This enables a more objective comparison to be made, as well as comparison with other numerical algorithms.

The first two problems are convection problems of a square wave [5] and a semicircle [6]. They can serve for the first comparisons of various numerical algorithms. Those giving unsatisfactory results should be abandoned. The third test problem is the two interacting blast waves problem [7]. It can serve for the comparison of numerical solutions of the complete hydrodynamic equations. Good

performance on such a difficult test problem should assure quality results under more ordinary circumstances.

3.1. *Convection of a Square Wave and a Semicircle*

The square wave convection test problem was introduced by Boris [5] for a basic comparison of various numerical algorithms. It involves the square wave travelling with a constant velocity. Though this test problem is very simple it can cause numerical difficulties to some algorithms due to the presence of steep gradients. These difficulties can show themselves as excessive numerical diffusion or as unphysical oscillations in the solution. The semicircle convection test problem was suggested by MacDonald [6] for further basic comparison of numerical algorithms. It involves the semicircle (half dome) travelling with a constant velocity. This test problem enables us to show the phase distortion effect for less diffusive algorithms and thus it represents an additional and finer convection test problem.

The convection problems require solution of the one-dimensional continuity equation (1). The initial conditions for both test problems are defined on a uniform grid of 100 points with periodic boundary conditions. Distance between grid points Δx is 1.0 m. The velocity $v = 1.0$ is constant within the whole system. Calculations are performed with three different time steps $\Delta t = 0.2$, 0.4, and 0.8 s, i.e., with the Courant numbers $\varepsilon = v\,\Delta t/\Delta x = 0.2$, 0.4, and 0.8, respectively.

The square wave is 20 grid points wide with constant density 2.0 from the 2nd to the 21st point. The density is 0.5 throughout the rest of the grid. The calculations are performed up to 160s; i.e., they require 800, 400, and 200 loops for respective time steps.

The semicircle is a total of 30 grid points wide with the density determined by

$$\rho_j = 1 + 2(1 - (j-20)^2/15^2)^{1/2} \tag{25}$$

from the 5th to the 35th point with a maximum of 3.0 at the 20th point. The density is 1.0 throughout the rest of the grid. The calculations are performed up to 60s; i.e., they require 300, 150, and 75 loops for the respective time steps.

The exact solution of the convection test problems is a shifted and unchanged initial density distribution. For more objective comparison of results, the average absolute error

$$\text{A.E.} = \frac{1}{100} \sum_j |\rho_j - \rho_j^{\text{exact}}| \tag{26}$$

will be used as a measure of inaccuracy of the solution gained numerically from the known exact solution.

3.2. *Two Interacting Blast Waves*

This test problem was introduced by Woodward [7] to illustrate the strong relationship between the accuracy of the overall flow solution and the thinness of

discontinuities on the grid. It involves multiple interactions of strong shocks, rarefactions, and contact discontinuities with each other and with boundaries. Because much of the important interactions take place in a small volume, this problem is very difficult to compute on a uniform Eulerian grid.

The test problem requires solution of the system of one-dimensional hydrodynamic equations,

$$\frac{\partial}{\partial t}(\rho)+\frac{\partial}{\partial x}(\rho v)=0 \tag{27}$$

$$\frac{\partial}{\partial t}(\rho v)+\frac{\partial}{\partial x}(\rho v^2)=-\frac{\partial}{\partial x}(p) \tag{28}$$

$$\frac{\partial}{\partial t}(E)+\frac{\partial}{\partial x}(Ev)=-\frac{\partial}{\partial x}(pv), \tag{29}$$

where ρ is the density, v is the velocity, p is the pressure, and E is the total energy density. This system of equations is closed by the expression for the total energy density

$$E=\frac{p}{\gamma-1}+\frac{1}{2}\rho v^2, \tag{30}$$

which serves for the determination of pressure. The initial condition consists of three constant states of an ideal gas with $\gamma=1.4$, which is at the rest between reflecting walls separated by a distance of 1 m. The density is 1.0 everywhere, while in the the leftmost tenth of the volume the pressure is 1000, in the rightmost tenth is 100, and in between it is 0.01. The resulting hydrodynamic flow evolution is relatively complex and details are given by Woodward and Colella [2].

Calculations are performed on two different grids of 200 and 800 points, i.e., with $\Delta x=0.005$ and 0.00125 m, respectively. The time step is variable and controlled such that the maximum Courant–Friedrichs–Lewy stability number

$$\varepsilon^*=(|v|+c)\frac{\Delta t}{\Delta x}, \tag{31}$$

where $c=(\gamma p/\rho)^{1/2}$ is the sound velocity, has approximately the same value during the whole calculation. The prescribed values used for $\varepsilon^*_{\max}$ are 0.4 and 0.8.

4. Results and Discussion

Here we present and discuss results of the given test problems. For more convenient comparison of the influence of our modifications, we present, at first, the results obtained using the original ETBFCT algorithm. Then we describe individual modifications and present the results obtained. All calculations were performed on the IBM 370/148 or the similar EC 1045 computer with the use of a single precision (32 bits in a word).

4.1. *Convection of a Square Wave*

Because the square wave moves on a periodic mesh, correct solution of this test problem by FCT algorithms requires not only periodic boundary conditions for densities but also some modifications within these algorithms. These modifications ensure correct periodic values also for transported and transported-diffused densities which are used as auxiliary quantities as well as ensuring correct action of the limiter at the boundaries. Figure 2 shows the solution of a square wave convection by the ETBFCT algorithm. The average absolute error (A.E.) is 0.0388 for $\varepsilon = 0.2$ which corresponds to the value of 0.038 given by Boris [3]. The possible small difference is caused by the different precision used for computation and by rounding errors. We have also used the ETBFCT algorithm with only "external" periodic boundary conditions (i.e., in its original form) when values of auxiliary quantities are obtained by extrapolation using the same gradients at boundaries as periodic densities have and when the limiter acts only partially. The solution obtained is only slightly more diffused with the average absolute error 0.0397. For comparison, the average absolute error is 0.260 for the Lax (or one-sided) algorithm, 0.119 for the double-step Lax–Wendroff algorithm with the added small diffusion, 0.057 for the first FCT algorithm SHASTA, and 0.042 (?) for the phoenical explicit LPE algorithm [5, 8]. Better results have been published [8] only for the phoenical implicit FCT, the reversible FCT, and the implicit optimal Fourier algorithms, with errors of 0.034, 0.033, and 0.022, respectively. However, these algorithms are not suitable for practical computations of shock waves [8]. Thus the ETBFCT gives the best published result gained by a general purpose algorithm. Accuracy of the solution increases for larger values of ε up to 0.5. Then the condition of monotonicity (9) is violated, because the diffusion introduced is not sufficient (Fig. 1). Though the solution is stable (7) it contains large overshoots and undershoots.

As has been mentioned in the previous section, linear numerical analysis shows that it is possible to realize the FCT algorithm which has ensured monotonicity for $|\varepsilon| \leqslant 1.0$ and thus it can use twice the time step rather than the ETBFCT algorithm. This algorithm has been named the XDFCT and it has formally the same order of amplitude and phase accuracy as the ETBFCT. The results of the square wave convection obtained by the XDFCT are shown in Fig. 3. It can be seen that the solution for $\varepsilon = 0.8$ is monotonic and has no overshoots or undershoots. For $\varepsilon \leqslant 0.5$, the average absolute errors are comparable with those of the ETBFCT. However,

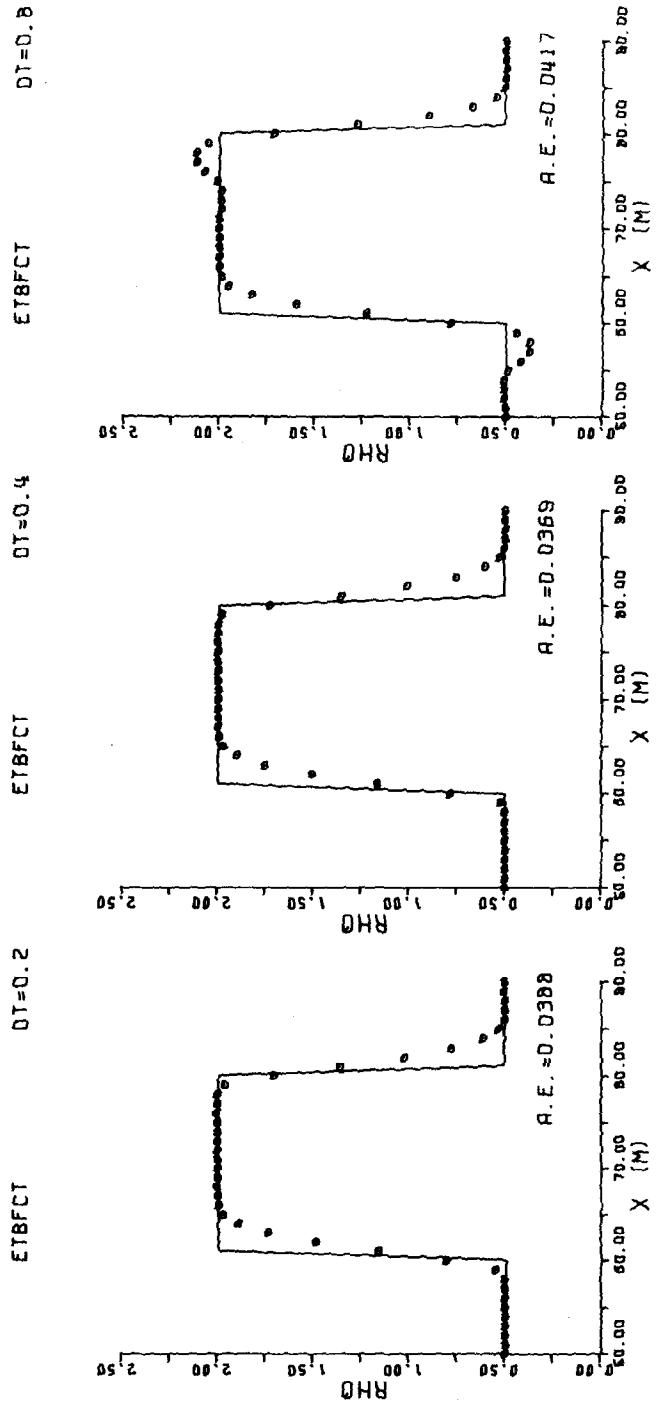

FIG. 2. Solution of the square wave convection problem by the ETBFCT at 160 s. Violation of the monotonicity can be seen for $\varepsilon = 0.8$. This can cause difficulties for the solution of hydrodynamic flow with steep gradients.

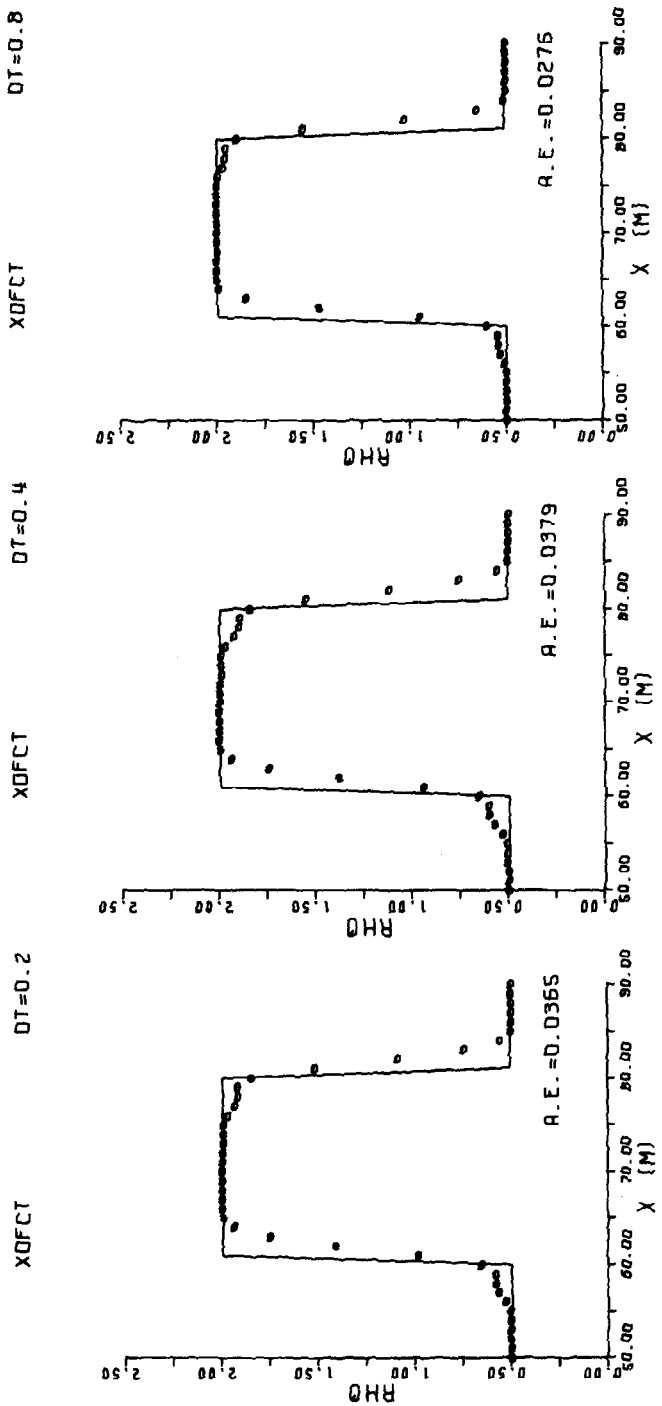

FIG. 3. *Solution of the square wave convection problem by the* XDFCT at 160 s. The reason for errors near wall edges is discussed in the text. Steeper gradients, however, result in average absolute errors comparable with those for the ETBFCT.

the XDFCT gives errors near the top edge at the beginning and behind the bottom edge at the end of the wave. These errors are caused by larger diffusion used at the main step which gives more "eroded" transported-diffused solution at steep gradients. This solution is used by the limiter for ensuring monotonicity during removal of excessive diffusion. Thus the applied antidiffusive fluxes are not allowed to fully remove the introduced excessive diffusion. Only the fact that the XDFCT gives more steep sides of the wave enables us to obtain comparable accuracy of the solution. This solution could be improved possibly by using a limiter which enables larger antidiffusive fluxes.

4.2. *Convection of a Semicircle*

Figure 4 shows the solution of a semicircle convection using the ETBFCT algorithm. Distortion of curved profiles can be seen. The semicircle profile has variable slopes between its values on the grid which can be considered as parts of waves with different wave lengths. Due to phase errors, these waves propagate, on a discrete grid, with different velocities and tend to steepen the profiles. This effect can be suppressed by larger diffusion which causes smoothing. However, the limiter does not detect this situation because no new extrema are formed or attenuated and thus it allows the removal of as much diffusion as possible. This results in distortion for less diffusive algorithms where phase errors are not overlayed or suppressed by amplitude ones. For $\varepsilon = 0.8$, the monotonicity condition (9) is violated; however, due to small gradients there are also small overshoots and undershoots. The phase distortion is smaller due to larger diffusion coefficients.

Finally, Fig. 5 shows the solution obtained using the XDFCT algorithm. Again the solution is monotonic for $\varepsilon = 0.8$. Errors caused by large diffusion used by the limiter (see the preceding subsection) are now small due to small gradients. All solutions are slightly more accurate than those obtained using the ETBFCT. This is caused by larger diffusion used by the limiter which is now welcome.

4.3. *Interaction of Two Blast Waves*

Figure 6 shows distribution of the density at times 0.026 and 0.038 s for the solution of the two interacting blast waves problem on 200 and 800 point grids with $\varepsilon^*_{\max} = 0.4$. Positions of the shocks and contact discontinuities are calculated very accurately. Further, the shock waves are sharply resolved with a width of only one cell. However, the contact discontinuities are slightly smeared. Especially, it is difficult to accurately resolve the contact discontinuity which originally formed at $x = 0.1$ m at times when it is overtaken by a reflected rarefaction wave with a steep density slope. Its position is approximately at 0.5 and 0.6 m in Figs. 6a and 6b, respectively. The hardest to represent is the compressed density slab between the contact discontinuity, which formed when the two shocks collided, and the contact discontinuity, which originally formed at $x = 0.9$ m. Its position is approximately between 0.65 and 0.8 m in Fig. 6b.

Figure 7 shows the solution obtained using the XDFCT algorithm on 200 and

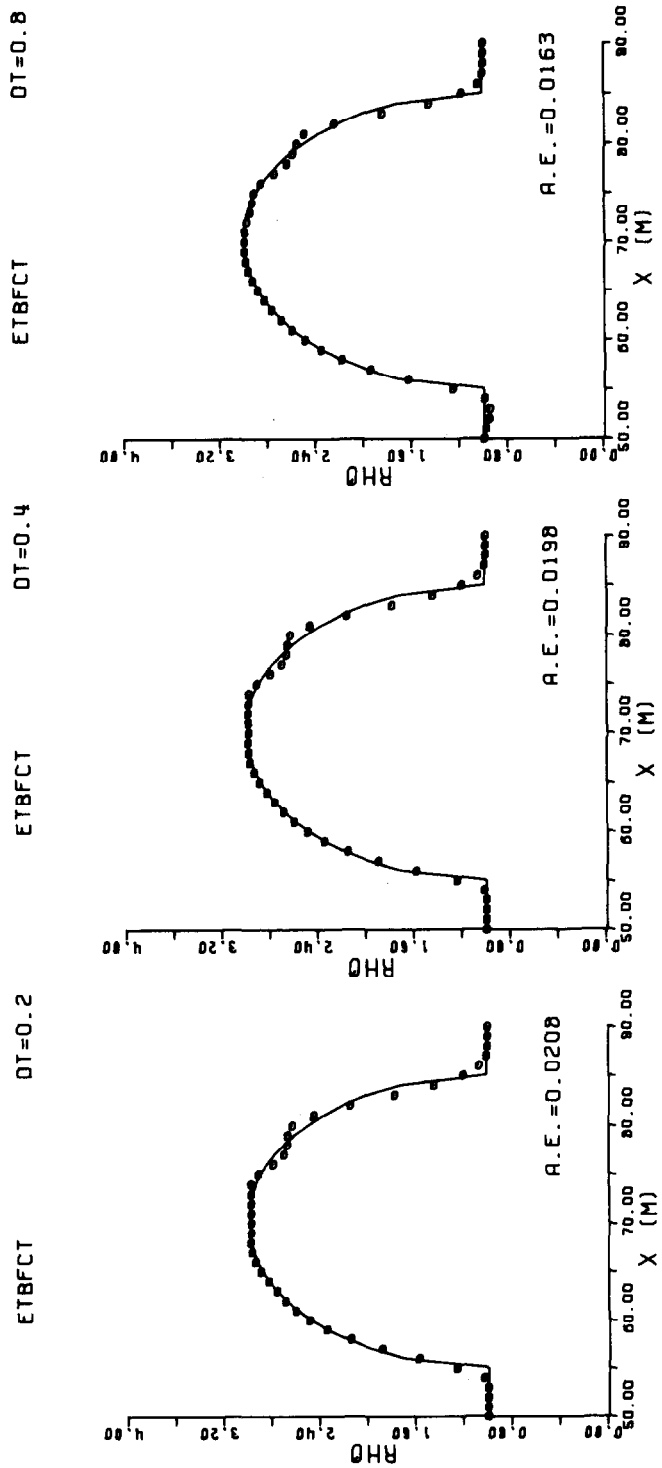

FIG. 4. Solution of the semicircle convection problem by the ETBFCT at 60 s. The reason for the distortion is discussed in the text. Small gradients cause only small violations of the monotonicity for $\varepsilon = 0.8$.

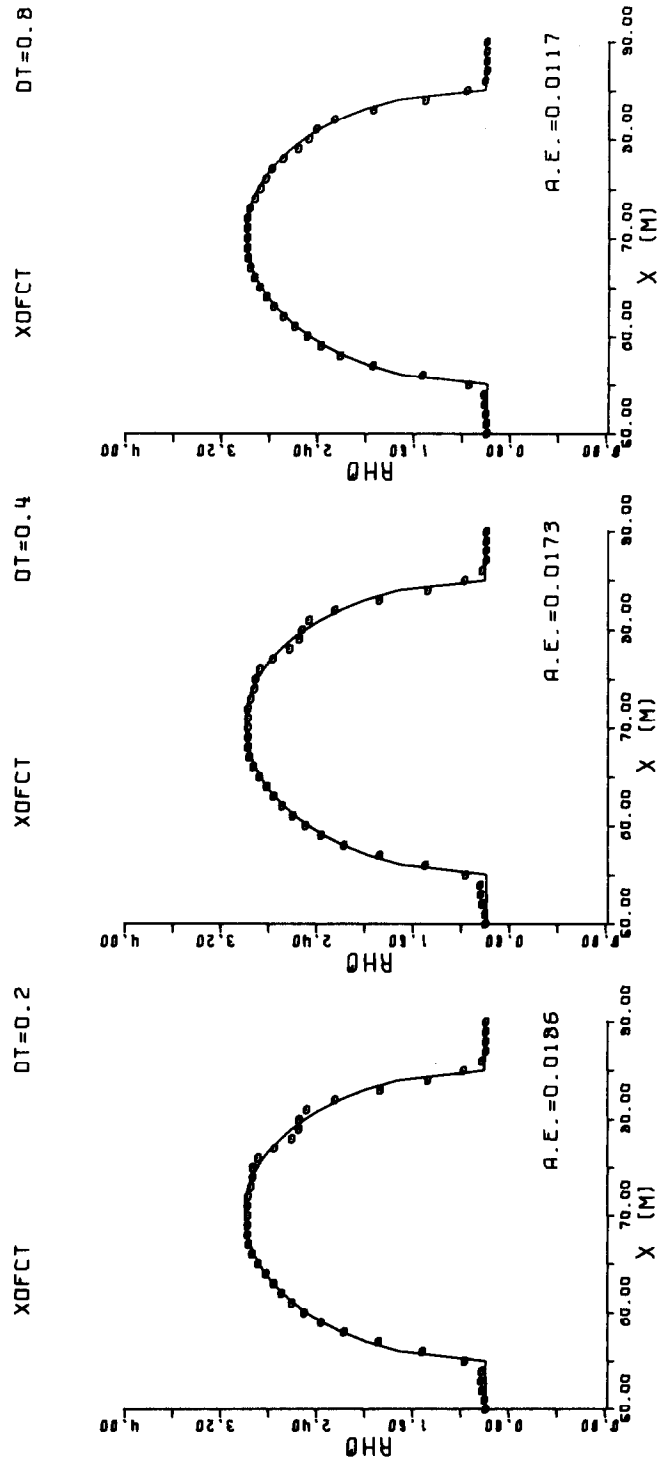

FIG. 5. Solution of the semicircle convection problem by the XDFCT at 60 s. The larger diffusion oefficients used enable us to obtain a slightly more accurate solution than with the ETBFCT.

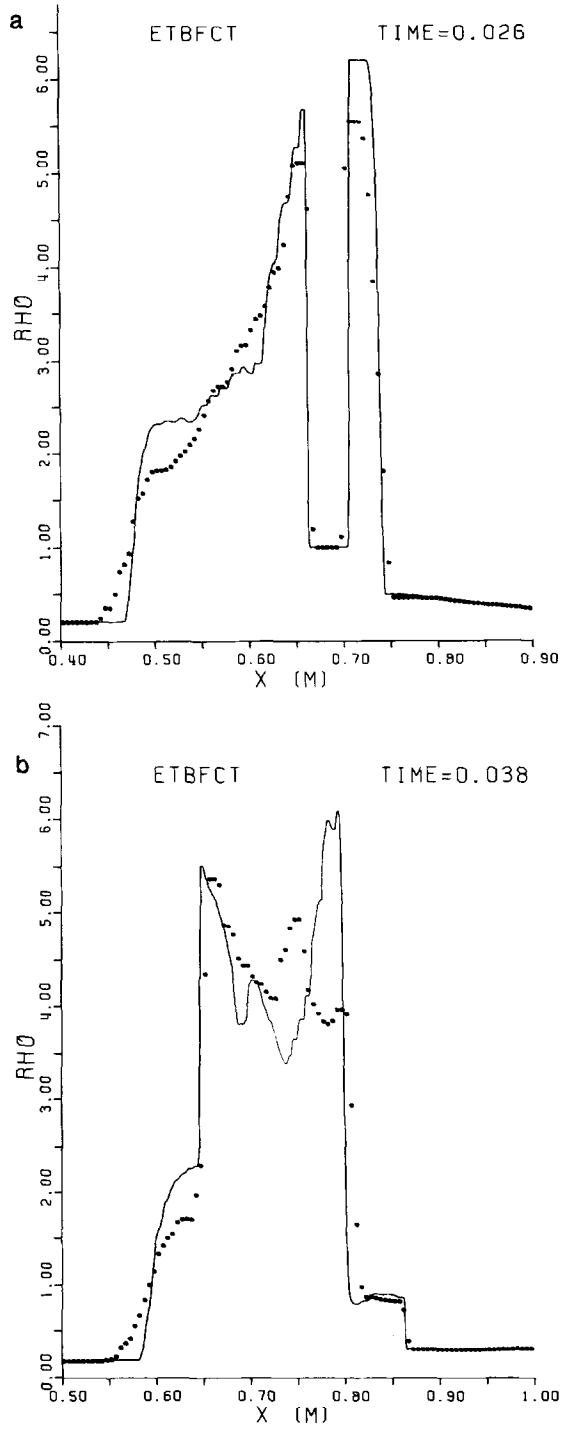

FIG. 6. Solution of the two interacting blast waves problem by the ETBFCT with $\varepsilon^*_{max} = 0.4$ on 200 point grid (circles) and 800 point grid (solid line) at 0.026 and 0.038 s. Calculation failed for $\varepsilon^*_{max} = 0.8$.

800 point grids with $\varepsilon^*_{max} = 0.8$. We note that the use of such large time steps caused the failure of calculation for the ETBFCT algorithm. The XDFCT solution is successful and comparable with that obtained using the ETBFCT with $\varepsilon^*_{max} = 0.4$. The XDFCT gives slightly lower density peaks on a 200 point grid, but slightly steeper contact discontinuities. Errors at steep gradients occur only for passively convected contact discontinuities and not for shock waves, and they are relatively very small for this extreme test. The solution on the 800 point grid is better for the ETBFCT between 0.55 and 0.6 m at 0.026 s and better for the XDFCT near 0.7 m at 0.038 s.

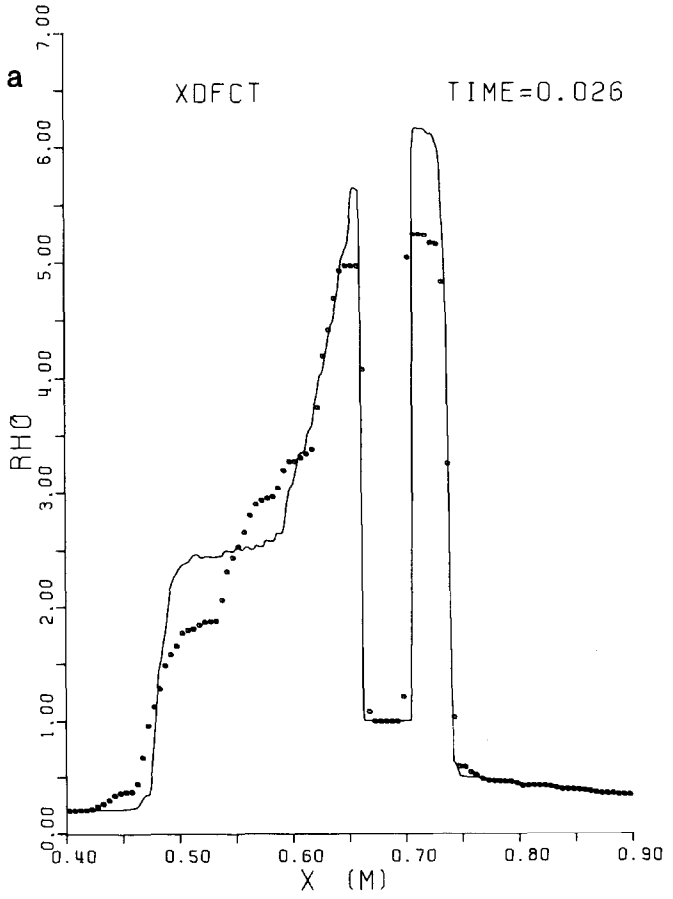

FIG. 7. Solution of the two interacting blast waves problem by the XDFCT with $\varepsilon^*_{max} = 0.8$ on 200 point grid (circles) and 800 point grid (solid line) at 0.026 and 0.038 s. Errors are relatively small for this extreme test.

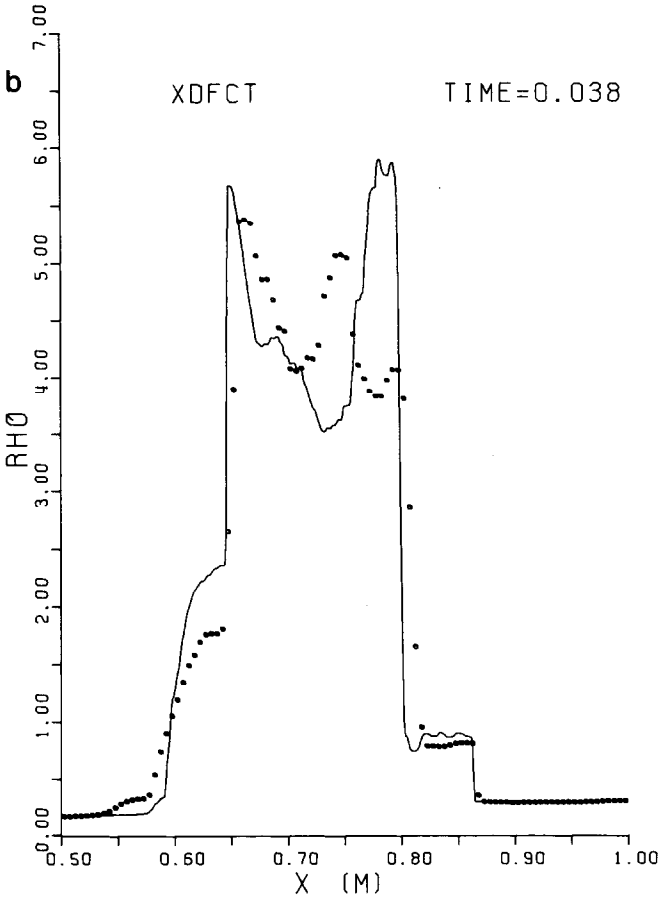

FIG. 7—*Continued*

5. CONCLUSIONS

We have introduced the XDFCT algorithm for solution of hydrodynamic flow with steep gradients. This algorithm is a modification of the existing ETBFCT algorithm and uses different antidiffusive fluxes. Optimal form of the corresponding diffusion and antidiffusion coefficients was found by linear numerical analysis. Amplitude and phase errors are reduced to the fourth order as in the ETBFCT; however, twice the time step can be used without violation of the monotonicity.

Three test problems were used to verify properties of the new algorithm. Solution of a square wave convection shows small errors near steep gradients. They are caused by larger diffusion coefficients which give the more diffused solution used by the limiter. This effect can be seen also in the hydrodynamic test problem for

contact discontinuities while shock waves are untouched except for slightly lower peaks. However, errors are relatively small in this extreme test. The solution at steep gradients could be improved by the limiter which allows larger antidiffusive fluxes. On the other hand, sides of a square wave and contact discontinuities are slightly steeper. Further, distortion of a semicircle convection is slightly smaller due to suppression of phase errors by higher diffusion coefficients. Use of twice the time step was successfully verified for all tests. The XDFCT makes it possible to reduce computer time for a given mesh or to gain higher resolution using a finer mesh for a given amount of computer time.

Appendix

Here we give details about the numerical analysis of the XDFCT algorithm. After each time step the numerical solution can be decomposed into a finite Fourier series. The behaviour of any given harmonic can be studied by substitution of

$$\rho_j^n = \hat{\rho}^n e^{ij\beta} \tag{A.1}$$

into the difference scheme, where $\hat{\rho}^n$ is the amplitude of the given harmonic and β is the phase angle ($\beta = k\,\Delta x = 2\pi\,\Delta x/\lambda$, where k is the wave number and λ is the wave length). The amplification function is defined as

$$g = \hat{\rho}^{n+1}/\hat{\rho}^n. \tag{A.2}$$

The relative amplitude error is defined as the amplitude of damping of the given harmonic

$$A = 1 - |g|^2, \tag{A.3}$$

where $|g|^2$, for complex function, is gg^* and g^* is the complex conjugate function of g. The relative phase error is defined as the difference of the distance propagated by the wave in the analytic solution and the distance propagated by the given harmonic in the numerical solution

$$R = \frac{x - v\,\Delta t}{v\,\Delta t} = \frac{kx}{\varepsilon\beta} - 1. \tag{A.4}$$

The value of x can be computed from

$$\tan(kx) = -\frac{\mathrm{Im}(g)}{\mathrm{Re}(g)}. \tag{A.5}$$

The amplitude and phase errors depend on ε, ν, μ, and β and for small β (i.e., large wave lengths), Taylor expansion can be used to find the optimal form of the diffusion and antidiffusion coefficients for minimizing these errors.

A.1. *Auxiliary Expressions*

Euler relations:

$$e^{i\beta} = \cos\beta + i\sin\beta, \tag{A.6}$$

$$e^{-i\beta} = \cos\beta - i\sin\beta. \tag{A.7}$$

Taylor expansions:

$$\sin\beta = \beta - \frac{\beta^3}{6} + \frac{\beta^5}{120} - \cdots, \tag{A.8}$$

$$\cos\beta = 1 - \frac{\beta^2}{2} + \frac{\beta^4}{24} - \cdots, \tag{A.9}$$

$$\arctan z = z - \frac{z^3}{3} + \frac{z^5}{5} - \cdots, \qquad |z| < 1, \tag{A.10}$$

$$\frac{1}{1-z} = 1 + z + z^2 + \cdots, \qquad |z| < 1. \tag{A.11}$$

A.2. *The Amplification Factor*

The XDFCT uses the difference scheme

$$\rho_j^{n+1} = \rho_j^n - \frac{\varepsilon}{2}(\rho_{j+1}^n - \rho_{j-1}^n) + N(\rho_{j+1}^n - 2\rho_j^n + \rho_{j-1}^n) - M(\rho_{j+1}^{n+1/2} - 2\rho_j^{n+1/2} + \rho_{j-1}^{n+1/2}), \tag{A.12}$$

where

$$\rho_j^{n+1/2} = \rho_j^n - \frac{\varepsilon}{4}(\rho_{j+1}^n - \rho_{j-1}^n) + \nu(\rho_{j+1}^n - 2\rho_j^n + \rho_{j-1}^n) - \mu(\rho_{j+1}^T - 2\rho_j^T + \rho_{j-1}^T) \tag{A.13}$$

and

$$\rho_j^T = \rho_j^n - \frac{\varepsilon}{4}(\rho_{j+1}^n - \rho_{j-1}^n). \tag{A.14}$$

Introducing (A.13) into the difference scheme gives

$$\rho_j^{n+1} = \rho_j^n - \frac{\varepsilon}{2}(\rho_{j+1}^n - \rho_{j-1}^n) + N(\rho_{j+1}^n - 2\rho_j^n + \rho_{j-1}^n)$$
$$- M\left[\rho_{j+1}^n - \frac{\varepsilon}{4}(\rho_{j+2}^n - \rho_j^n) + \nu(\rho_{j+2}^n - 2\rho_{j+1}^n + \rho_j^n)\right.$$
$$\left. - \mu(\rho_{j+2}^{\mathrm{T}} - 2\rho_{j+1}^{\mathrm{T}} + \rho_j^{\mathrm{T}})\right]$$
$$+ 2M\left[\rho_j^n - \frac{\varepsilon}{4}(\rho_{j+1}^n - \rho_{j-1}^n) + \nu(\rho_{j+1}^n - 2\rho_j^n + \rho_{j-1}^n)\right.$$
$$\left. - \mu(\rho_{j+1}^{\mathrm{T}} - 2\rho_j^{\mathrm{T}} + \rho_{j-1}^{\mathrm{T}})\right]$$
$$- M\left[\rho_{j-1}^n - \frac{\varepsilon}{4}(\rho_j^n - \rho_{j-2}^n) + \nu(\rho_j^n - 2\rho_{j-1}^n + \rho_{j-2}^n)\right.$$
$$\left. - \mu(\rho_j^{\mathrm{T}} - 2\rho_{j-1}^{\mathrm{T}} + \rho_{j-2}^{\mathrm{T}})\right] \tag{A.15}$$

which is

$$\rho_j^{n+1} = \rho_j^n - \frac{\varepsilon}{2}(\rho_{j+1}^n - \rho_{j-1}^n) + (N-M)(\rho_{j+1}^n - 2\rho_j^n + \rho_{j-1}^n)$$
$$+ \frac{M\varepsilon}{4}(\rho_{j+2}^n - 2\rho_{j+1}^n + 2\rho_{j-1}^n - \rho_{j-2}^n)$$
$$- M\nu(\rho_{j+2}^n - 4\rho_{j+1}^n + 6\rho_j^n - 4\rho_{j-1}^n + \rho_{j-2}^n)$$
$$+ M\mu(\rho_{j+2}^{\mathrm{T}} - 4\rho_{j+1}^{\mathrm{T}} + 6\rho_j^{\mathrm{T}} - 4\rho_{j-1}^{\mathrm{T}} + \rho_{j-2}^{\mathrm{T}}). \tag{A.16}$$

Further, introducing (A.14) gives

$$\rho_j^{n+1} = \rho_j^n - \frac{\varepsilon}{2}(\rho_{j+1}^n - \rho_{j-1}^n) + (N-M)(\rho_{j+1}^n - 2\rho_j^n + \rho_{j-1}^n)$$
$$+ \frac{M\varepsilon}{4}(\rho_{j+2}^n - 2\rho_{j+1}^n + 2\rho_{j-1}^n - \rho_{j-2}^n)$$
$$- M\nu(\rho_{j+2}^n - 4\rho_{j+1}^n + 6\rho_j^n - 4\rho_{j-1}^n + \rho_{j-2}^n)$$
$$+ M\mu\left(\rho_{j+2}^n - \frac{\varepsilon}{4}(\rho_{j+3}^n - \rho_{j+1}^n)\right) - 4M\mu\left(\rho_{j+1}^n - \frac{\varepsilon}{4}(\rho_{j+2}^n - \rho_j^n)\right)$$
$$+ 6M\mu\left(\rho_j^n - \frac{\varepsilon}{4}(\rho_{j+1}^n - \rho_{j-1}^n)\right) - 4M\mu\left(\rho_{j-1}^n - \frac{\varepsilon}{4}(\rho_j^n - \rho_{j-2}^n)\right)$$
$$+ M\mu\left(\rho_{j-2}^n - \frac{\varepsilon}{4}(\rho_{j-1}^n - \rho_{j-3}^n)\right), \tag{A.17}$$

which is

$$\rho_j^{n+1} = \rho_j^n - \frac{\varepsilon}{2}(\rho_{j+1}^n - \rho_{j-1}^n) + (N-M)(\rho_{j+1}^n - 2\rho_j^n + \rho_{j-1}^n)$$
$$+ \frac{M\varepsilon}{4}(\rho_{j+2}^n - 2\rho_{j+1}^n + 2\rho_{j-1}^n - \rho_{j-2}^n)$$
$$- M(\nu-\mu)(\rho_{j+2}^n - 4\rho_{j+1}^n + 6\rho_j^n - 4\rho_{j-1}^n + \rho_{j-2}^n)$$
$$- M\mu\frac{\varepsilon}{4}(\rho_{j+3}^n - 4\rho_{j+2}^n + 5\rho_{j+1}^n - 5\rho_{j-1}^n + 4\rho_{j-2}^n - \rho_{j-3}^n). \quad \text{(A.18)}$$

Now, substitution of (A.1) into this difference scheme enables us to gain the amplification function

$$g = 1 - \frac{\varepsilon}{2}(e^{i\beta} - e^{-i\beta}) + (N-M)(e^{i\beta} + e^{-i\beta} - 2)$$
$$+ \frac{M\varepsilon}{4}(e^{i2\beta} - e^{-i2\beta} - 2e^{i\beta} + 2e^{-i\beta})$$
$$- M(\nu-\mu)(e^{i2\beta} + e^{-i2\beta} - 4e^{i\beta} - 4e^{-i\beta} + 6)$$
$$- M\mu\frac{\varepsilon}{4}(e^{i3\beta} - e^{-i3\beta} - 4e^{i2\beta} + 4e^{-i2\beta} + 5e^{i\beta} - 5e^{-i\beta}). \quad \text{(A.19)}$$

Introducing trigonometric functions (A.8)–(A.9) gives

$$g = 1 - \varepsilon i \sin\beta + 2(N-M)(\cos\beta - 1)$$
$$+ \frac{M\varepsilon}{2}(i\sin 2\beta - 2i\sin\beta) - 2M(\nu-\mu)(\cos 2\beta - 4\cos\beta + 3)$$
$$- M\mu\frac{\varepsilon}{2}(i\sin 3\beta - 4i\sin 2\beta + 5i\sin\beta), \quad \text{(A.20)}$$

which is finally

$$g = 1 - 2(N-M)(1-\cos\beta) - 2M(\nu-\mu)(\cos 2\beta - 4\cos\beta + 3)$$
$$- i\varepsilon\left[\left(1 + M + \frac{5}{2}M\mu\right)\sin\beta - \left(\frac{M}{2} + 2M\mu\right)\sin 2\beta + \frac{M\mu}{2}\sin 3\beta\right]. \quad \text{(A.21)}$$

A.3. *The relative Amplitude Error*

The modulus of the amplification function (A.21) is

$$|g|^2 = [1 - 2(N-M)(1-\cos\beta) - 2M(\nu-\mu)(\cos 2\beta - 4\cos\beta + 3)]^2$$
$$+ \varepsilon^2\left[\left(1 + M + \frac{5}{2}M\mu\right)\sin\beta - \left(\frac{M}{2} + 2M\mu\right)\sin 2\beta + \frac{M\mu}{2}\sin 3\beta\right]^2. \quad \text{(A.22)}$$

Expanding trigonometric functions (A.8)–(A.9) gives

$$|g|^2=\left[1-2(N-M)\left(1-1+\frac{\beta^2}{2}-\frac{\beta^4}{24}\right)\right.$$
$$\left.-2M(\nu-\mu)\left(1-\frac{4\beta^2}{2}+\frac{16\beta^4}{24}-4-\frac{4\beta^2}{2}+\frac{4\beta^4}{24}+3\right)\right]^2$$
$$+\varepsilon^2\left[\left(1+M+\frac{5}{2}M\mu\right)\left(\beta-\frac{\beta^3}{6}\right)\right.$$
$$\left.-\left(\frac{M}{2}+2M\mu\right)\left(2\beta-\frac{8\beta^3}{6}\right)+\frac{M\mu}{2}\left(3\beta-\frac{27\beta^3}{6}\right)\right]^2, \tag{A.23}$$

which is

$$|g|^2=\left[1-(N-M)\,\beta^2-\left(M(\nu-\mu)-\frac{N-M}{12}\right)\beta^4\right]^2+\varepsilon^2\left[\beta-\left(\frac{1}{6}-\frac{M}{2}\right)\beta^3\right]^2. \tag{A.24}$$

The relative amplitude error (A.3) is then

$$A=[2(N-M)-\varepsilon^2]\,\beta^2$$
$$+\left[-(N-M)^2-\frac{N-M}{6}+2M(\nu-\mu)+\frac{1}{3}\varepsilon^2-M\varepsilon^2\right]\beta^4+\cdots. \tag{A.25}$$

A.4. *The Relative Phase Error*

The phase properties are derived from

$$\tan(kx)=\frac{\varepsilon[(1+M+5M\mu/2)\sin\beta-(M/2+2M\mu)\sin 2\beta+(M\mu/2)\sin 3\beta]}{1-2(N-M)(1-\cos\beta)-2M(\nu-\mu)(\cos 2\beta-4\cos\beta+3)}. \tag{A.26}$$

Expanding trigonometric functions (A.8)–(A.9) gives

$$\tan(kx)=\frac{\left(\begin{array}{l}\varepsilon[(1+M+5M\mu/2)(\beta-\beta^3/6)-(M/2+2M\mu)(2\beta-8\beta^3/6)\\ \quad+(M\mu/2)(3\beta-27\beta^3/6)]\end{array}\right)}{\left(\begin{array}{l}1-2(N-M)(1-1+\beta^2/2)\\ \quad-2M(\nu-\mu)(1-4\beta^2/2-4+4\beta^2/2+3)\end{array}\right)}, \tag{A.27}$$

which is

$$\tan(kx)=\frac{\varepsilon\beta[1+(-\frac{1}{6}+M/2)\,\beta^2]}{1-(N-M)\,\beta^2}. \tag{A.28}$$

Use of the inverse function and its expansion (A.10) gives

$$kx = \frac{\varepsilon\beta[1+(-\frac{1}{6}+M/2)\,\beta^2]}{1-(N-M)\,\beta^2} - \frac{\varepsilon^3\beta^3/3[1+(-\frac{1}{6}+M/2)\,\beta^2]^3}{[1-(N-M)\,\beta^2]^3}. \tag{A.29}$$

The relative phase error (A.4) is then

$$R = \frac{\begin{pmatrix} -[1-(N-M)\,\beta^2]^3 + [1+(-\frac{1}{6}+M/2)\,\beta^2][1-(N-M)\,\beta^2]^2 \\ -\varepsilon^2\beta^2/3[1+(-\frac{1}{6}+M/2)\,\beta^2]^3 \end{pmatrix}}{[1-(N-M)\,\beta^2]^3}. \tag{A.30}$$

Considering terms only up to the order of β^2 gives

$$R = \frac{-1+3(N-M)\,\beta^2+1+(-\frac{1}{6}+M/2)\,\beta^2-2(N-M)\,\beta^2-(\varepsilon^2/3)\,\beta^2}{1-3(N-M)\,\beta^2}, \tag{A.31}$$

which is

$$R = \left(N-\frac{M}{2}-\frac{1}{6}-\frac{\varepsilon^2}{3}\right)\beta^2\frac{1}{1-3(N-M)\,\beta^2}. \tag{A.32}$$

Expanding fraction (A.11) and again considering terms only up to the order of β^2 finally gives

$$R = (N-M/2-\tfrac{1}{6}-\tfrac{1}{3}\varepsilon^2)\,\beta^2 + O(\beta^4) + \cdots. \tag{A.33}$$

ACKNOWLEDGMENTS

The author thanks E. S. Oran for drawing his attention to the semicircle test problem. A large set of various computations were performed for this work which was possible thanks to the kind services of computer centres at the Slovak Academy of Sciences, the Slovak Planning Committee, and the Institute for Economy and Organization of Civil Engineering.

REFERENCES

1. J. P. BORIS AND D. L. BOOK, "Solution of Continuity Equations by the Method of Flux-Corrected Transport," in *Methods in Computational Physics*, Vol. 16, edited by J. Killeen (Academic Press, New York, 1976).
2. P. WOODWARD AND P. COLELLA, *J. Comput. Phys.* **54**, 115 (1984).
3. J. P. BORIS, NRL Memorandum Report No. 3237, 1976 (unpublished).
4. D. L. BOOK, J. P. BORIS, AND S. T. ZALESAK, "Flux-Corrected Transport," in *Finite-Difference Techniques for Vectorized Fluid Dynamics Calculations*, edited by D. L. Book (Springer-Verlag, New York, 1981).
5. J. P. BORIS AND D. L. BOOK, *J. Comput. Phys.* **11**, 38 (1973).
6. E. S. ORAN AND J. P. BORIS, "Continuity Equation: Eulerian Methods," *Numerical Simulation of Reactive Flow* (Elsevier, New York, 1987).
7. P. WOODWARD, "Comparison of Various Explicit Hydrodynamic Schemes for Vector Computers," in *Parallel Computations*, edited by G. Rodrigue (Academic Press, New York, 1982).
8. J. P. BORIS AND D. L. BOOK, *J. Comput. Phys.* **20**, 397 (1976).